Extreme Mechanics Letters 52 (2022) 101681

Contents lists available at ScienceDirect

Extreme Mechanics Letters

journal homepage: www.elsevier.com/locate/eml

Auxetic boosting of confinement in mortar by 3D reentrant truss lattices for next generation steel reinforced concrete members

Georgios Tzortzinis [a], Andrew Gross [b], Simos Gerasimidis [c,*]

[a] Dresden Center for Intelligent Materials (DCIM), Technische Universität Dresden, Germany
[b] Department of Mechanical Engineering, University of South Carolina, Columbia, SC, United States of America
[c] Department of Civil and Environmental Engineering, University of Massachusetts, Amherst, MA, United States of America

ARTICLE INFO

Article history:
Received 29 October 2021
Received in revised form 26 February 2022
Accepted 27 February 2022
Available online 8 March 2022

Keywords:
Auxetic materials
Reinforced concrete
Interpenetrating phase composites
Reentrant truss lattices

ABSTRACT

A study is presented on a new method for confining concrete/mortar materials using steel auxetic truss lattice reinforcement. The study builds on major advances in architected materials and a new concept for the confinement of structural members. Numerical results are presented on a unit cell of the new composite including a mortar matrix and a steel reentrant auxetic lattice as reinforcement, followed by a small scale experimental phase where 3D printed steel auxetic lattices are encased in mortar and tested under axial compression. Several findings emerge: the auxetic lattice applies enhanced confinement to the mortar matrix, the new composite exhibits significant strength increase compared to plain mortar specimens and the composite has a remarkably ductile behavior, with a high residual strength that endures to strains in excess of 20%. The experimental results are further validated through computational modeling. The findings of this paper demonstrate the high potential of using auxetic lattices as reinforcement in a concrete/mortar matrix with advantageous properties for structures in terms of strength and ductility which are crucial in the response of structures under extreme loading conditions such as earthquakes.

1. Introduction

Fundamental mechanics together with manufacturing and materials science advancements have led to the creation of architected materials (or mechanical metamaterials) with mechanical properties that are not found in naturally occurring materials. The novel architectures that enable these unique material properties also provide extensive tunability of the properties through variations in geometry. Most architected materials that have been fabricated exhibit at least one attribute that is incompatible with structural and infrastructure applications (e.g. high cost from additive manufacturing, fabrication with methods that are difficult to scale up, or the use of raw materials that do not meet typical cost and performance expectations). Thus far, these associations have largely prevented their adoption in structural and infrastructure applications, yet opportunities to dramatically improve the performance and sustainability of the built environment with compatible architected materials present themselves. In addition, emerging digital automated fabrication methods using robotics or additive manufacturing at the structural scale are expected to soon allow the manufacturing of architected materials for structural applications.

The construction industry is the top user of materials in terms of volume of materials needed, and concrete is by far the most used material; concrete is the most widely used material in the world after water with about 2 billion tons used per year [1]. In terms of mechanical performance, typical plain concrete under axial compressive stress experiences the formation and growth of microcracks which in turn constitute a "damage" process that eventually leads to brittle failure [2]. This process is demonstrated by the non-linear softening response under uniaxial compressive loading and Early work by Richart [3] has demonstrated the effectiveness of lateral confinement on improving the behavior of concrete under axial compressive stresses. It is widely known that lateral confinement can be used to delay concrete failure and significantly improve its ductility which is highly desirable for structures under extreme loads such as earthquakes [4].

Today, there are two main techniques used to confine concrete: active and passive confinement. Confinement in the form of internal discontinuous transverse reinforcement bars or external steel jackets and fiber reinforced polymer (FRP) jackets are used to delay the damage process by restraining the dilation of concrete (see Fig. 1a). This type of confinement is passive in nature as the transverse reinforcement is activated by the lateral dilation of concrete due to its positive Poisson's ratio. Because of its beneficial effect, there have been numerous studies and systematic experimental tests in the last 50 years on the behavior of

* Corresponding author.
E-mail address: sgerasimidis@umass.edu (S. Gerasimidis).

https://doi.org/10.1016/j.eml.2022.101681
2352-4316/

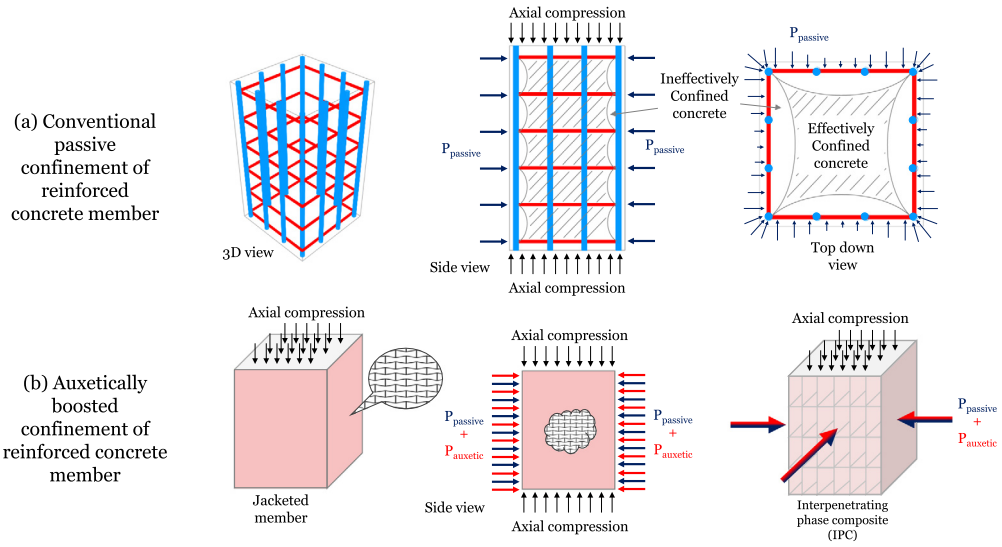

Fig. 1. Schematic concept of the auxetically confined composite: (a) A reinforced concrete (RC) column passively confined using conventional steel transverse reinforcement bars (in red), (b) a concrete column confined using an auxetic jacket or an interpenetrating phase composite of concrete and an open-cell auxetic network. The confinement pressure is a combination of passive confinement and auxetically-induced confinement. (For interpretation of the references to color in this figure legend, the reader is referred to the web version of this article.)

concrete confined by transverse reinforcement. The compressive stress–strain curve and the properties of the compressive stress block of flexural members were proposed by Kent and Park [5]. Sheikh and Uzumeri [6] focused on the strength and ductility of tied concrete columns testing 24 square columns. They showed that when concrete is confined using regular ties and longitudinal reinforcement, it can exhibit a significant strength gain of up to 70%, as well as increased ductility. Scott et al. [7] also performed an experimental program of 25 columns reaching similar results while another experimental program by Park and Priestley [8] reported the benefits of transverse reinforcement on the ductility of concrete. Mander et al. [9], after conducting a study on concrete columns, proposed a stress–strain model that has been widely used by many researchers. However, as pointed out in [9,10], the effectiveness of passive confinement strongly depends on the area of the concrete where the confining stress is fully developed. As shown in Fig. 1a, confining concrete through transverse reinforcement leads to the development of a 3D arching action and therefore the volume of the effectively confined concrete is less than the volume of the total concrete in a structural member. Alternatively, new techniques such as the application of active confinement have emerged in recent years toward an effort to reach higher performance of reinforced concrete (RC) structures. Active confinement is the process of applying external confining pressure on a concrete element before loading [11]. Experimental, computational and theoretical contributions have presented the effect of shape memory alloys on the confinement of concrete cylinders demonstrating the effectiveness of this process [12,13]. However, this technique comes with many practical limitations in terms of high cost, extensive labor and handling of complex equipment for prestressing and, therefore, its application has been limited [14].

Auxetic truss-lattices are a particularly well studied subset of architected materials, which are materials whose behavior is dominated by an engineered arrangement of matter (and void space), rather than the largely stochastic microstructures of traditional materials. Their maturity stems from a broader interest in auxetic materials on account of their high shear stiffness [15,16], fracture toughness [17], energy absorption [18–20], indentation resistance [21,22], and fatigue life [23,24]. The amount of benefit is problem specific, e.g. in [24] it was found that an auxetic design could extend the fatigue life a massive 160 times longer than that of a non-auxetic, while in [16] the increase of shear stiffness for the auxetic over non-auxetic design is more modest at 43 percent. There are two avenues for achieving auxetic behavior in truss-lattices — the use of reentrant cells was demonstrated first [25,26], whereas the use of chiral cells came later [27].

Recent technological advances have greatly expanded the types of architected materials that can be engineered and the range of mechanical properties that can be achieved. Composite materials consisting of multiple phases have been used for producing extremal bulk modulus [28], negative coefficient of thermal expansion [29,30], and negative Poisson's ratio [31,32]. Among these composites, interpenetrating phase composites (IPCs) belong to a distinct family in which each constituent phase forms a completely interconnected three-dimensional network. It is due to the continuous morphology that each constituent contributes its property to the overall macro scale characteristics synergistically. For example, if one constituent provides negative Poisson's ratio (auxeticity) the other might enhance stiffness or strength. These materials can also be found in nature such as in skeletal tissue and botanical systems [33]. The geometry and topology of the constituents provide avenues to engineer the macroscale properties of IPCs.

Numerous IPCs have been developed and now exist in the literature with remarkable properties [33–39]. A recent study [33] examines the feasibility of processing lightweight syntactic foam based IPCs and has found that the increase in the plateau stress of IPC foam samples is about eight times that of an unfilled preform. The effective elastic properties of metal–ceramic IPCs have been investigated and included in [36]. Valuable results on characterizing IPCs formed by combining a polymer with metal foam are provided in [40] showing improvements in elastic properties as high as 50%.

IPCs utilizing lattice architectures have demonstrated enhanced mechanical performance achieving a unique combination of stiffness, strength and energy absorption [37]. A new method for increasing the ductility of ultra-high-performance concrete by reinforcing it with 3D printed polymeric octet lattice lattices was recently presented in [41]. In recent studies [42,43] a class of high-performance composites was reported in which auxetic lattice structures have been used as reinforcement within

a soft matrix using additive manufacturing techniques. It was shown that harnessing the negative Poisson's ratio effect using 2D in-plane auxetic reinforcement, the soft matrix enters a state of biaxial compression improving the mechanical response. Another study presented computational results showing potential in energy absorption when encasing auxetic lattices as reinforcement in concrete [44].

To create next generation reinforced concrete for structural components, we pattern internal steel reinforcements to form an auxetic network that generates confining pressure even without lateral expansion of the surrounding matrix (see Fig. 1b). To achieve this, we use auxetic truss-lattices to develop a new class of high-performance mortar that harnesses auxetically boosted confinement. This augmented confinement is generated first as a result of the mechanical properties of the embedded reinforcement which stem from its auxetic architectural pattern, as well as from the passive activation of the steel lattices due to the dilation of the mortar (see Fig. 1b). Besides the confinement boosting due to the auxetic nature of the lattice, another major advantage of the auxetically boosted confinement is that contrary to conventional confinement reinforcement (see Fig. 1b) which has a 1D periodicity, the auxetic lattice has a periodicity in 3D and as a result the new auxetically boosted confinement mechanism is able to avoid the weakest link failure which happens in conventional confinement when a hoop fractures [7]. First, we perform linear finite element method (FEM) simulations to characterize the confinement pressures of an auxetic steel architected material within a mortar matrix. For this specific material combination, we find that reinforcements that maximize matrix confinement do so through a combination of passive and auxetically induced components. Then, we 3D print the steel auxetic architectures and we embed them in a mortar matrix to perform small scale experiments. The recorded stress–strain curves show repeatable confinement behavior with excellent ductility and residual strength due to the auxetic reinforcement. The auxetically confined specimens exhibit substantial strength increase at small strains and tremendous deformation capacity while maintaining strength above unconfined strength. The strength gain because of the confinement is between 2.4–2.5 compared to the unconfined mortar, which is a substantial strength increase. Finally, the experimental results are validated with nonlinear FEM simulations of the auxetic composite.

Overall, our results demonstrate that the concept of auxetically boosted confinement can be used to increase the mechanical properties of reinforced concrete in terms of confinement, strength and ductility.

2. Modeling

2.1. Geometry

A series of truss lattices using the architecture proposed in [45] are investigated. The characteristic angle θ of the architecture was varied in steps of 5 degrees from 70 to 135 degrees to generate reentrant and convex lattices (see Fig. 2a). Within each lattice, every strut is given the same length l and diameter d. The strut aspect ratio of l/d is unique for each characteristic angle θ and was selected so that every lattice has a relative density of $\bar{\rho} = 0.05$, since this is a typical volume fraction of steel reinforcement used in reinforced concrete structural members (see Fig. 2b). This results in a tetragonal unit cell, with aspect ratio $\Lambda = \frac{a_z}{a_x}$. A small fillet with a radius of $d/4$ was added at the strut intersections. To make an IPC, the void space within the unit cell of the truss lattice is replaced with solid material. A perfect bond between the lattice and matrix were assumed.

2.2. Unit cell models

The elastic properties of the truss lattice materials and their IPC counterparts are calculated by simulating deformations on unit cell models using the finite element method (ABAQUS/Standard). The base materials for the truss are assumed to have an elastic modulus of $E^{(T)} = 200$ GPa and a Poisson's ratio of $\nu^{(T)} = 0.3$. To model a steel lattice in mortar, the matrix is assumed to have an elastic modulus of $E^{(M)} = 2806$ MPa and Poisson's ratio $\nu^{(M)} = 0.18$ for IPC models. All models use tetrahedral elements with quadratic shape functions (C3D10). Each bare truss model makes use of approximately 40,000 elements and approximately 200,000 elements are used in the IPC models. Periodic boundary conditions are applied via equation constraints that were created with a python script. Macroscopic strains corresponding to nine orthogonal states of uniaxial, equibiaxial, and shear strains were applied and the associated strain energy was used to compute the nine required elastic constants for orthotropic materials following the procedure outlined in [46]. Only the small deformation elastic behavior was considered in these simulations, thus material and geometric nonlinearities are not accounted for.

2.3. Analytical modeling

A Voigt model is used to estimate the properties of the IPC from the compliance tensors of the two phases. The orthotropic compliance tensor of the truss lattice is calculated with the FE unit cell models, whereas the matrix is assumed to be isotropic. The decrease in matrix stiffness from the small volume that the lattice occupies is calculated according to the Hashin–Shtrikman bound. The two phases are subjected to uniaxial compressive stress in the z-direction and are required to have identical strain components. In this situation, the applied load is split between the two phases as:

$$\frac{\sigma_{zz}^{(M)}}{\sigma_{zz}^{(T)}} = \frac{s_{33}^{(T)}}{s_{33}^{(M)}} + \left(\frac{s_{13}^{(M)} + s_{23}^{(M)} + s_{13}^{(T)} + s_{23}^{(T)}}{s_{33}^{(M)}}\right)\frac{\sigma_0}{\sigma_c} \tag{1}$$

Where σ_c is the applied stress, σ_0 is the transverse stress, and s are components of the compliance tensor. The superscripts (M) and (T) indicate quantities for the matrix and truss, respectively. The ratio between the transverse stress σ_0 and applied stress σ_c depends on the mismatch between the two phases according to:

$$\frac{\sigma_0}{\sigma_c} = \frac{s_{13}^{(M)}s_{33}^{(T)} - s_{13}^{(T)}s_{33}^{(M)}}{s_{33}^{(M)}\left(s_{11}^{(M)} + s_{12}^{(M)} + s_{11}^{(T)} + s_{12}^{(T)}\right) - s_{13}^{(M)}\left(s_{13}^{(M)} + s_{23}^{(M)} + s_{13}^{(T)} + s_{23}^{(T)}\right)} \tag{2}$$

Finally, the confining pressure in the matrix, $p^{(M)}$, can be calculated as:

$$\frac{p^{(M)}}{\sigma_c} = \frac{1}{3}\left(2\frac{\sigma_0}{\sigma_c} - \frac{\sigma_{zz}^{(M)}}{\sigma_{zz}^{(T)}}\right) \tag{3}$$

To separate the effect of Poisson's ratio from lateral stiffness, a second set of IPC's with modified truss lattice properties were investigated using this same approach. The modified truss lattice properties are taken to have the same elastic moduli as the original lattices, but the Poisson's ratios are set equal to zero (i.e. $s_{ij}^{(T)} = 0$ for $i \neq j$). The confining pressure in the matrix calculated with the modified truss lattice properties is from the effect of transverse stiffness alone, and the difference between the two pressure calculations is due to the truss having non-zero Poisson's ratio.

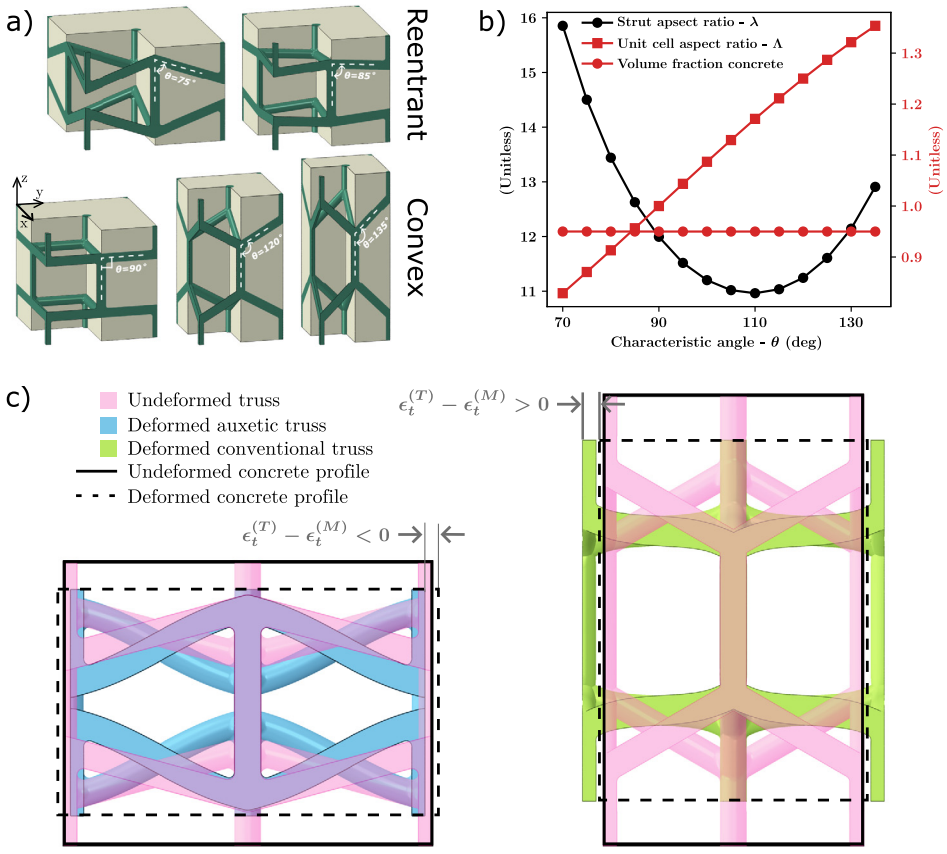

Fig. 2. (a) IPC's with reentrant and convex truss lattice reinforcement. (b) Strut and unit cell aspect ratios for truss lattices with a relative density of $\bar{\rho} = 0.05$. (c) Undeformed and deformed shapes of reentrant and convex bare truss lattices in comparison to the same for mortar. Opposing deformation of the reentrant truss lattice is indicated by a negative mismatch strain.

2.4. Unit cell results

The effect of negative Poisson's ratio is observable in Fig. 2c by lateral contraction of the reentrant lattice when axially compressed. This contraction opposes the lateral expansion of pure mortar in compression, which has a Poisson's ratio $\nu^{(M)} = 0.18$. The mismatch in transverse deformation can be quantified by subtracting the lateral strain of the mortar from that of the truss lattice. As the mismatch strain $\epsilon_m = \epsilon_t^{(T)} - \epsilon_t^{(M)}$ becomes more negative, the lattice is expected to exert more force squeezing the surrounding mortar (assuming that lattice stiffness remains constant). Confinement of the mortar can then be enhanced from classical passive steel reinforcement, where $\epsilon_m \geq -\epsilon_t^{(M)}$, by using lattices that are auxetic. Following the same rationale, convex lattices (which when subjected to uniaxial compression exhibit lateral expansion) are expected to degrade the confinement of mortar due to an increase of the mismatch strain ϵ_m (illustrated in Fig. 2c).

All truss lattice materials considered in the design space have a coordination number $z = 5$ and are bending dominated. When subjected to compressive uniaxial stress in the z-direction, all struts that are not parallel to the z-direction undergo bending (Fig. 3a). The bending deformation of these struts persists in IPC's with convex reinforcement (with some attenuation from the matrix). Different behavior emerges for auxetic truss lattice materials, since the bending deformation opposes the behavior of the matrix. As a result, the lattice becomes stretching dominated and carries tensile stress in members that are not parallel to the direction of loading (Fig. 3b). This tension in the reinforcement must be balanced by lateral compression in the matrix, since the average lateral stress of both phases must still sum to zero. This is observable in the pressure field of the matrix, where it can be seen that the auxetic lattice produces more confining pressure (Fig. 3c).

The dependence of select elastic properties on the characteristic angle θ are shown in Fig. 3d for the bare truss. The moduli are normalized by the product of the parent material's modulus and the relative density:

$$\bar{E}^* = \frac{E^*}{\bar{\rho} E^{(T)}}$$

Where E^* is an elastic modulus of the bare truss. The lattice is auxetic for $\theta < 90°$, with a monotonically increasing Poisson's ratio. The axial modulus is nearly zero for the most auxetic lattice ($\bar{E}_z^* = 0.00690$) and also increases monotonically to a modest normalized value of $\bar{E}_z^* = 0.124$ for $\theta = 135°$. The transverse modulus exhibits non-monotonic behavior, with a maximum value of $\bar{E}_x^* = 0.461$ at a characteristic angle $\theta = 90°$. The transverse modulus is very sensitive to the characteristic angle in this neighborhood, and is roughly symmetric about $\theta = 90°$.

The same three properties are shown in Fig. 3e when the lattice is encased in mortar to make an IPC. The moduli of the IPC are normalized by that of mortar. The trend for transverse modulus is quite similar to that of the bare truss lattice, but with reduced variation between the maximum and minimum values. The axial modulus exhibits a different trend than the bare truss lattice, slightly decreasing for characteristic angles $70° < \theta < 95°$ and then increasing after the minimum at $\theta = 95°$. This non rule of mixtures response is a further reflection of the switch from bending to stretching domination for auxetic lattices embedded in a matrix. None of the IPC's are auxetic, but the Poisson's ratio

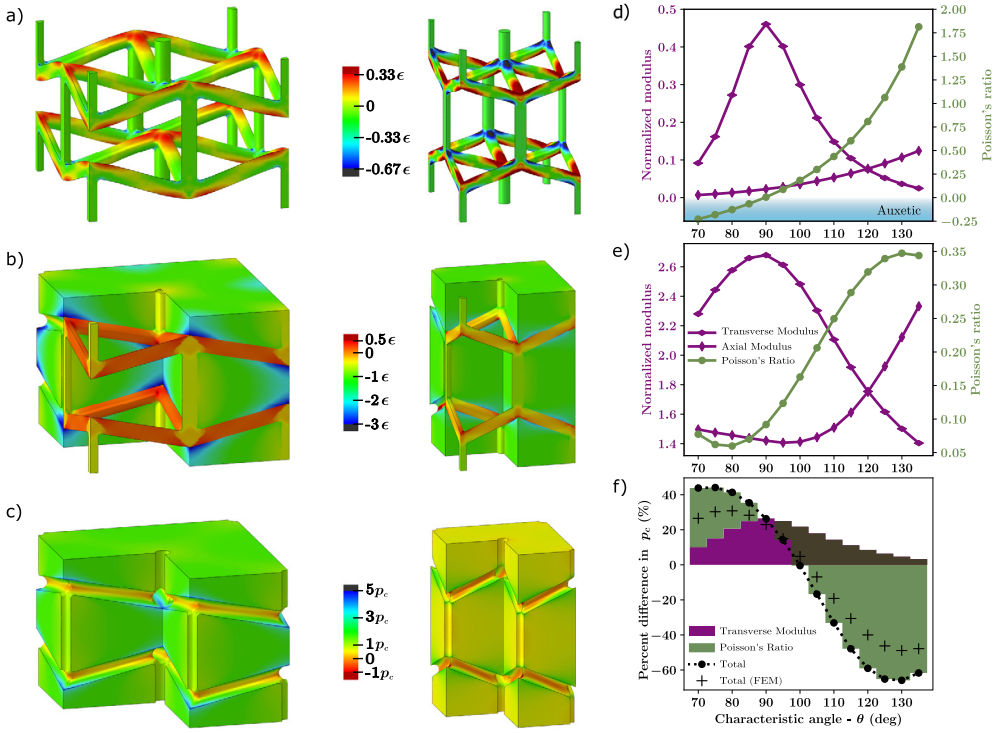

Fig. 3. Max magnitude principal strain contours on reentrant ($\theta = 80°$) and convex ($\theta = 120°$) (a) bare truss lattices and (b) corresponding IPC's when subjected to compressive uniaxial stress in the z-direction to cause an average axial strain with magnitude ϵ. Uniform strain within the struts of the reentrant lattice in (b) indicate stretch dominated deformation. (c) Confining pressure contours in the matrix relative to the confining pressure in pure mortar, p_c. Matrix and lattice are removed from portions of figures (b) and (c) for clarity. Poisson's ratio and normalized elastic moduli for bare truss lattices (d) and IPC's (e). (f) Effect on confining pressure relative to pure mortar. Confinement from lateral stiffness and Poisson effect are decomposed for the analytical model, while only total results are available from FE unit cell models.

is less than that of the matrix for characteristic angles $\theta < 105°$. The minimum Poisson's ratio is found for a characteristic angle of $\theta = 80°$, which is also the characteristic angle where the greatest confining pressure is produced (Fig. 3f).

The influence of the reinforcement on the total confining pressure predicted by the analytical model is overstated due to the Voigt assumption, however the overall trend is very similar to the FE unit cell model results (Fig. 3f). The analytical model is used to decompose the contributions to the confining pressure from lateral stiffness and Poisson's ratio of the truss lattice. The contribution from lateral stiffness exhibits the same trend as the transverse modulus in Figs. 3d–e, attaining its maximum value at $\theta = 90°$. For reinforcement lattices with $\theta < 90°$, the negative Poisson's ratio enhances the confining pressure during compressive loading, supplying more confining pressure than is lost to the decrease in transverse stiffness until the characteristic angle $\theta = 75°$. The general agreement between analytical and FE unit cell models clearly indicates that the maximum confining pressure at $\theta = 80°$ calculated by the FE unit cell models is also due to contributions from the lateral stiffness and negative Poisson's ratio of the truss lattice. Notably, these results elucidate a new mechanism of producing confining pressure and show that its contribution can be sizeable in comparison to traditional passive confinement. The analytical model also confirms the deleterious effect on confinement from reinforcement lattices with a positive Poisson's ratio ($\theta > 90°$) when the material is subjected to uniaxial compression.

These results also provide insight on the initial (linear) behavior of the IPC when subjected to uniaxial tensile loading by multiplying the values in Figs. 3a–c and 3f with negative one. With this modification in mind, Fig. 3f then shows that both the transverse stiffness and Poisson effect from the auxetic lattice unfavorably reduce the confining pressure when compared to the case of unreinforced matrix material subjected to tensile loading. Thus, the auxetic lattice is expected to have a deleterious effect if used in regions of a structure with tensile loading. Note that regardless of whether a lattice is reentrant or convex, its transverse stiffness always has an unfavorable effect on the confining pressure in tensile loading. Remarkably, the Poisson effect from convex lattices is strong enough to overcome the effect from transverse stiffness and produce a substantial net increase of confining pressure when subjected to tensile loading (an enhancement of 48.9% for $\theta = 130°$ is predicted from the FE unit cell model). Thus, a pathway to extend the current results for uniaxial loading to structures subjected to bending loads is apparent. Functional grading of the characteristic angle θ for the lattice is expected to be advantageous when the reentrant and convex lattices are used on the compressive and tensile sides of the neutral axis, respectively.

3. Experimental testing and validation

3.1. Sample fabrication

Steel auxetic lattices were fabricated and encased in a mortar matrix to experimentally validate the confinement effect of the auxetic lattice on the matrix. To achieve this goal, auxetically confined mortar specimens were fabricated using a $4 \times 4 \times 4$ tessellation of a $\theta = 85°$ reentrant steel auxetic truss-lattice architecture, embedded in a mortar cubic volume with edge length equal to 50.8 mm. To maintain the reinforcement volume fraction equal to 5%, which corresponds to a typical design of a reinforced concrete member under compression, the strut diameter was set equal to 1.003 mm. Two families of vertical struts with aspect ratios equal to 7.34 and 5.31 are included in the architecture to achieve a cubic unit cell. The characteristic angle $\theta = 85°$

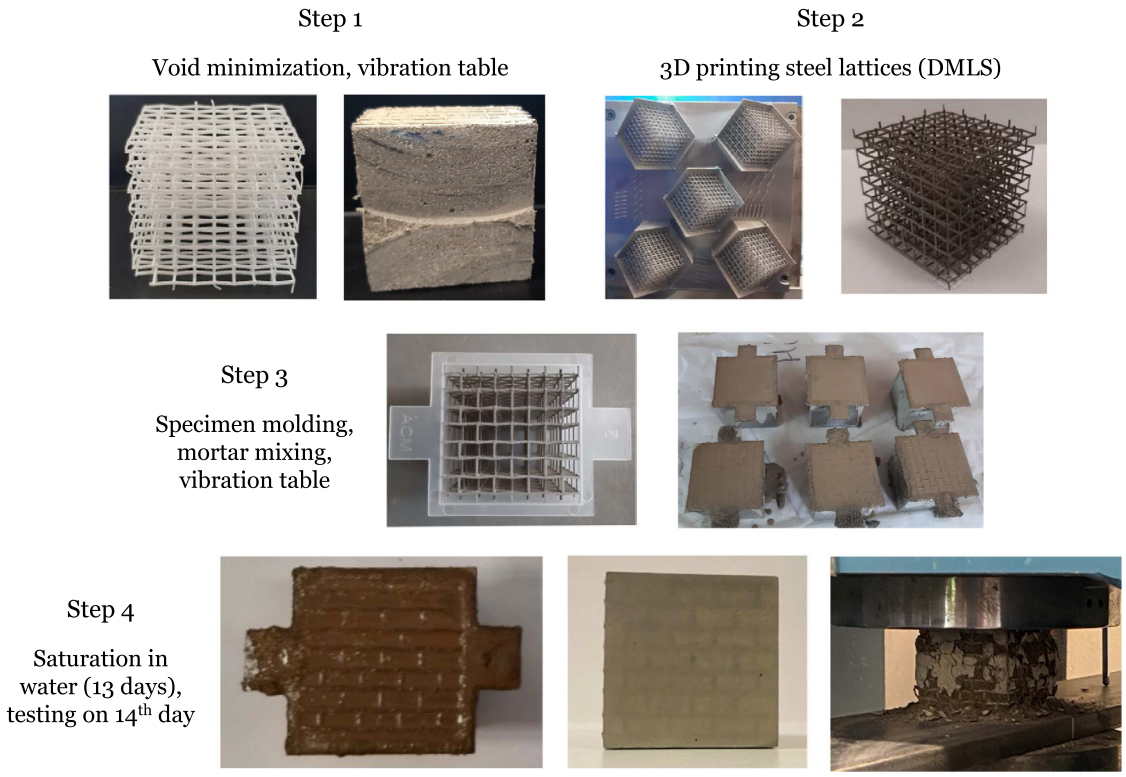

Fig. 4. Fabrication process of the auxetically confined mortar specimens. Step 1: Polymer lattices used to find the appropriate vibration protocol to minimize voids after pouring. The photo shows a cross-section of a specimen including a polymer lattice using the vibration protocol, Step 2: 3D printing of the steel auxetic lattices, Step 3: Steel auxetic lattices in the cubic molds right after the pouring, Step 4: The molds were saturated in water for 13 days and the tests were performed on the 14th day.

was selected from the angles expected to produce high confining pressures on the mortar.

The lattices were fabricated with pre-alloyed steel powder [47] based on the DMLS (Direct Metal Laser Sintering) technology, where, laser heating melts particulate feedstock to fuse them together. EOS StainlessSteel PH1 powder was used in an EOSINT M 270. A layer thickness of 20 μm was used. The nominal yield strength of the produced metal is 1050 ± 50 MPa and 1000 ± 50 MPa in the build plane and perpendicular to it, respectively. The corresponding ultimate tensile strengths are 1150 ± 50 MPa and 1050 ± 50 MPa, along the same directions. The mortar's composition was based on ASTM Standards [48] with 1 part cement and 2.75 parts of sand proportioned by mass. Based on the same set of recommendations, portland cement is employed with water–cement ratio of 0.485. However, the proposed mixture was slightly modified to better serve the purposes of the experiment. Initially, the maximum grain size was set equal to 0.71 mm, while a plasticizer was used to increase the flowability of the mortar between the lattice struts and at the same time to reduce the potential creation of voids in the matrix. To maintain the water–cement ratio constant to 0.485, 22 mL of water were replaced with equal quantity of admixture. The final composition for a batch is presented in Table 1.

The composite specimens were prepared in cubic molds with 50.8 mm long edge. A thin coating of release agent was applied to the interior faces of the molds before the latices are fitted in position. The lattices were embedded in the molds such that the compressive loading surface would be perpendicular to the casting face to ensure that no protruding parts result to stress concentration. Hand tamping could not be applied due to the dense reinforcement mesh, thus a vibration table was chosen as an alternative consolidation method. Considering that there is not an established procedure for the vibration table, within the frame of cement mortars, we carried out a series of preparatory tests to conclude on a combination of mortar layers and vibration time, able to result in consistent compressive capacities. Initially, polymer lattices with architecture identical to the steel geometries were manufactured (Fig. 4, Step 1). Employing the mortar composition, illustrated in Table 1, sets consisted of three specimens each, were prepared from each batch. Tests were performed, to conclude in a procedure that provides capacities which do not deviate more than 8.7% of the average when three cubes represent a test age [48]. Additional composite specimens were prepared and sliced to ensure that no significant voids are detected between the struts in the lattices (Fig. 4, Step 1). The results indicated that the mortar would be poured in 4 equally thick layers, and vibration would be activated for 30 s at the end of each deposition. Immediately upon completion of molding, the specimens were placed in a moist room for 24 h. Subsequently, the specimens were removed from the molds and were saturated in water for additional 13 days to assist cement strengthening (Fig. 4, Step 3). Finally, the tests were performed on the 14th day after molding (Fig. 4, Step 4).

Table 1
Composition of mortar matrix in which the auxetic lattices were encased. A plasticizer has been used to ensure the flowability of the mortar matrix through the auxetic lattices to avoid voids in the composite.

	Proposed by [48]	This work
Cement (g)	500	500
Sand (g)	1375	1375
Water (mL)	242	220
Plasticizer (mL)	–	22

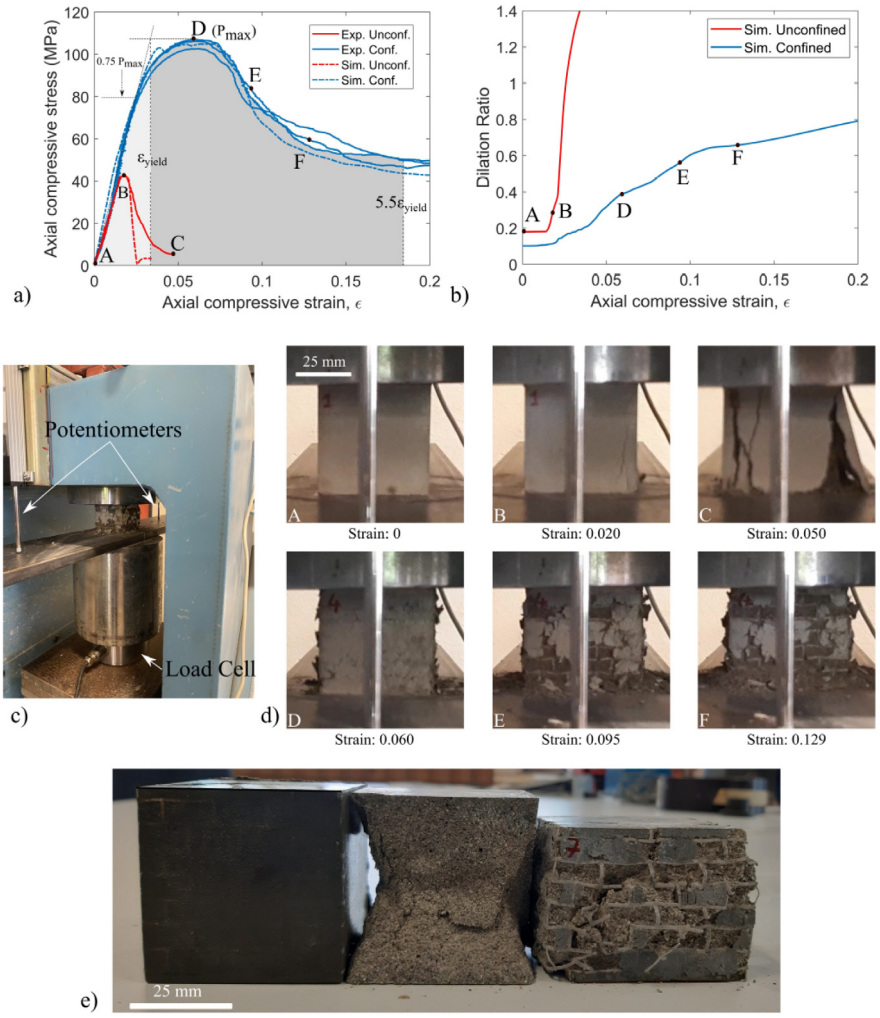

Fig. 5. Experimental results: (a) Stress–strain curves of the three auxetically confined mortar specimens and the plain mortar specimen. With dashed lines, the results of the computational validation are also included. (b) Evolution of the dilation ratios in the confined and unconfined specimens (simulations). (c) The test set-up including the locations of the two potentiometers, (d) deformation of an unconfined specimen (A, B and C) and an auxetically confined specimen (D, E and F) at different strains during the experiment and (e) residual deformations of an unconfined, and a confined specimen in comparison with the as-built dimensions. Buckling and failure within the truss-lattice can be observed in the confined specimen, as well as extensive mortar cracking.

3.2. Mechanical testing

Each specimen was subjected to monotonically increasing displacement-controlled compression. A load cell was installed above the fixed specimen's top surface to record the applied load. Strains were calculated by the average of displacement recordings obtained by two potentiometers with repeatability of 0.002 mm (Fig. 5).

3.3. Experimental results

One baseline specimen with plain mortar and three IPC specimens were prepared and tested. The repeatability of the fabrication process is achieved using the protocol described above and the peak compressive strength of the mortar is found to be 42 MPa which is consistent with the literature in mortar [49]. The performance of the specimens under compression is evaluated based on the peak load, the corresponding strain, and the post-peak behavior. The obtained axial stress–strain response is presented in Fig. 5a, while Figs. 5d and 5e illustrate the residual deformations of an unconfined, and a confined specimen in comparison with the as-built dimensions.

The stress–strain behavior of the IPC is found to be repeatable, with a consistent ultimate load and post-peak response at high levels of deformation. Compared to the unconfined mortar specimen, the peak load of the IPC specimens are 139%–149% higher than the unconfined mortar specimen. Additionally, the strain at peak load for the IPC specimens is increased by up to 221% in comparison to unconfined mortar. This increase in strength is attributed to the role of the auxetic lattice in the confinement of the specimen which comes along with a remarkable increase by 340% in the allowable axial strain. The large observed strains are one of the most interesting attributes of the composite which appears to be in contrast to conventional confining methods of concrete. However, this finding would need to be validated for actual concrete specimens in a larger scale. Another interesting observation can be made about the mode of failure at the peak load. As expected, the plain mortar specimen fails by the typical sharp cone mode shown in Fig. 5e. On the other hand, the auxetically confined composite specimens are held together for strains exceeding 3.4 times the strain at peak load, presented in Fig. 5d (C, D, E). The majority of cracks observed from images taken during the testing (Fig. 5d) are limited to the thin outer layer of mortar cover. The ductility performance of the IPC specimens is measured according to the ductility index I_{10}, proposed by Foster and Attard [50]. The ductility index is calculated as the ratio of the area under the axial compressive load–axial strain

curve up to $5.5\epsilon_{yield}$, where ϵ_{yield} is the yield strain. The yield strain is found using the 3/4 method by extending a line from the origin of the graph crossing $0.75P_{max}$ until P_{max}. The ductility indices of the three IPCs are found to be 7.4, 7.6, 7.7 which are considered to provide significant ductility [51,52]. Although these results show great promise regarding the ductility index, further experiments with concrete and auxetic lattices fabricated from conventional steel rebar should be performed for direct comparisons to reinforced concrete structures.

The IPC specimens exhibit exceptionally repeatable post-peak behavior with a residual strength at strains up to 20% that remain higher than the peak-strength of the unconfined mortar specimen. Fig. 5e presents the auxetically confined specimen after the completion of the test, revealing that at large axial strains the specimen has remained together although there are fractured or buckled struts in the auxetic lattice. This phenomenon is in contrast to conventionally confined concrete members where the axial capacity of a member is catastrophically reduced after the first perimetric hoop fracture [7]. The 3D distribution of members in the auxetic lattice throughout the mortar allows the redistribution of stresses throughout the whole volume of the composite, providing significant redundancy to local strut failures. This is a benefit of 3D periodicity in the placement of reinforcement material, so that structural members made of the architected material do not suffer from weakest link type failure.

Looking forward, as this auxetic confinement method moves to concrete members, this attribute is extremely valuable, as the ductility of confined concrete structural members is one of the most important properties for the design of structures to extreme events such as earthquakes. The ability of the mortar IPC specimen to absorb energy by retaining high strength through large axial strains shows great promise for reaching ductility levels that are unprecedented with the current confinement methods. More experimental and computational work would be required to explore the ductility of the auxetically confined concrete at the structural scale.

3.4. Computational validation

The experimental results are validated through FEM using a dynamic explicit model (ABAQUS/Explicit). The auxetic truss is simulated using linear Timoshenko beam elements (B31) and the mortar using linear hexahedron solid elements with reduced integration (C3D8R). The truss-lattice was assembled as a 3D assembly entity in Abaqus and it was embedded into the mortar solid elements using the embedded region constraint. The host elements were the solid elements simulating the mortar and the embedded elements were the Timoshenko beam elements of the auxetic truss-lattice. The mesh of the model is defined such that there are 15,000 beam elements and 185,000 solid elements to accurately capture the behavior. The same elastic properties used in the unit cell analysis are used for the mortar. In addition, the density of the mortar is 2288 kg/m^3, while a concrete damaged plasticity model based on [53] has been adopted for the failure using a dilation angle of 25°, flow potential eccentricity 0.1, $f_{b0}/f_{c0} = 1.16$ and $k = 0.666$; where f_{b0}/f_{c0} is the ratio of initial equibiaxial compressive yield stress to initial uniaxial compressive yield stress and k is the ratio of the second stress invariant on the tensile meridian. The compressive and tensile behavior have been adopted from the plain mortar specimens and introduced into the simulations. For the steel auxetic lattice, a density of 7800 kg/m^3, a modulus of $E^{(T)} = 200$ GPa and a Poisson's ratio of $\nu^{(T)} = 0.3$ have been used. The plastic flow of the steel has been defined as 1000 MPa at 0 plastic strain, 1100 MPa at 0.16 plastic strain and 150 MPa at 0.2 plastic strain which is compatible to the values of the steel powder used during the 3D printing. The stress–strain curves of the computational models for the unconfined mortar as well as the auxetically confined mortar specimens are presented with dashed lines in Fig. 5a, validating the experimental results.

In addition, the computational simulation of the composite structure has provided results on the dilation ratio of the confined and the unconfined specimens which are shown in Fig. 5b. As presented in the graph, the dilation ratio of the unconfined specimen starts from 0.18 as expected, but very soon rises dramatically due to the failure of the specimen. On the other hand, the dilation ratio of the auxetically confined specimen starts from 0.1 which is close to what had been calculated in the linear calculation (see Fig. 3e). The difference between the elastic calculation which provides a smaller Poisson's ratio for the composite than the nonlinear computation is attributed to the periodic boundary conditions which are not part of the experimental validation computations and also to the beam simulation of the auxetic lattice in the nonlinear simulation. Nevertheless, the dilation ratios between the two calculations are reasonably close. Furthermore, the evolution of the dilation ratio of the confined specimen presents the effect of the auxetic lattice used for the confinement by delaying the dilation of the confined specimen and the dilation ratio plateaus at a value around 0.8 which is considerably low. This attribute of the auxetically boosted confinement is particularly important as it distinguishes this method from passive confinement; in passive confinement a dramatic failure is observed after the fracture of one of the transverse hoop reinforcements [7]. In addition, when compared to active confinement, the evolution of the dilation ratio for auxetically boosted confinement exhibits lower values which is beneficial.

3.5. Comparison of auxetic lattice to a conventional confinement configuration

To assess the superiority of the auxetic lattice in the confinement of the mortar and its effect on the strength and the ductility of the member, the validated computational model was used to perform analysis using a conventional confinement configuration. The comparison of the auxetic lattice to a conventional passive confinement technique is a critical comparison which can provide necessary evidence about the advantages of the auxetic lattice.

To achieve that, a typical passive confinement configuration for members under compression was adopted consisting of longitudinal bars and transverse hoop reinforcement (perimetrical and rhombical), as shown in Fig. 6. This type of passive confinement can also be found in Fig. 1 of [7]. The conventional confinement includes 12 longitudinal bars of 1.45 mm radius, perimetrical hoops of 0.7 mm radius and rhombical hoops of 0.7 mm spaced at 6 mm. The spacing of the transverse perimetrical and rhombical hoops was reduced by one-half at each end of the test unit to provide extra reinforcement at the ends and ensure that the failure would occur in the central region of the specimen avoiding the effect of the boundary conditions, as this configuration is not periodic in 3D as the auxetic one [7]. The overall volume of steel material between the auxetic lattice and the passive conventional configuration is identical to ensure a meaningful comparison.

The results shown in Fig. 6 demonstrate the superiority of the auxetic lattice both in terms of strength and in terms of ductility. Compared to the unconfined mortar specimen, the peak load of the conventional passive configuration is increased by around 70%. However, this increase is much lower than the 140% increase when the auxetic lattice is used to confine the mortar. Further, as also found in [7], the pre-peak behavior is characterized as linear and the failure of the conventionally confined member is rather sudden and brittle, while the auxetically confined members exhibited a nonlinear behavior close to the peak load and

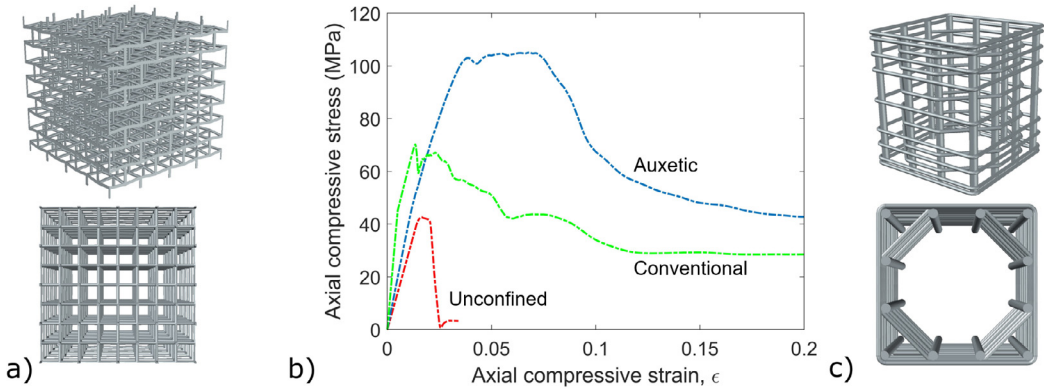

Fig. 6. (a) Reentrant lattice used for the auxetically confined model, (b) Computationally derived stress–strain curves of unconfined (red), conventionally confined (green) and auxetically confined (blue) members under compression demonstrating the significant increase in strength and ductility when the auxetic lattice is used for confining the member, (c) Conventional passive confinement configuration. (For interpretation of the references to color in this figure legend, the reader is referred to the web version of this article.)

the failure can be characterized as more ductile. The failure of the conventional member is attributed to the sudden buckling of the longitudinal bars in the central region and between the transverse hoops, followed by the yielding of the hoops. Post-peak, the conventionally confined member follows a degradation at lower stresses, when compared to the descending branch of the auxetically confined member, illustrating the significantly lower ductility properties of the conventionally confined mortar.

4. Conclusions

A new confinement method for reinforcing cementitious materials for structural applications has been presented using an auxetic lattice as reinforcement in a mortar matrix. In contrast to conventional confinement methods which are generally passive in nature (resisting the lateral expansion of concrete under axial loading), the new confinement strategy takes advantage of the unique behavior of auxetic lattices to laterally contract under compressive axial loading. Linear finite element unit cell models show that the auxetic behavior causes the lattice to transition from bending to stretching dominated behavior, with struts transverse to the direction of compressive loading are placed in tension, thereby increasing confinement of the matrix. Analytical modeling has shown that the confinement of mortar by a steel lattice is maximized when passive and auxetically induced confinement work together. Finite size nonlinear finite element modeling and experimental results reveal remarkably repeatable damage behavior of the steel/mortar composite when subjected to large deformations. The new confinement strategy increases compressive strength by 140% and exhibits ductile post-peak behavior with a residual strength that exceeds the peak strength of unconfined mortar – even to strains as large as 20%. The new reinforced material is resilient, and retains this high load carrying capability even after local failure of steel struts in the lattice occur. The small scale experimental study shows great promise for reinforced concrete members with unprecedented strength, ductility and energy absorption. These new results along with the rapid advances in automated digital fabrication of lattices in the structural scale can be the building blocks for the next generation of reinforced concrete structures. Although using additive manufacturing for steel lattices in the structural scale is currently cost-prohibitive, advances in the technology could render this solution as possible in the future. In addition, robotic fabrication techniques for bending, assembling and welding could be used as alternative manufacturing techniques to achieve cost effective solutions.

Declaration of competing interest

The authors declare that they have no known competing financial interests or personal relationships that could have appeared to influence the work reported in this paper.

Acknowledgments

This work was partially supported by the National Science Foundation, United States of America (Grant No. CAREER CMMI-2044705) and startup funding from the University of South Carolina, United States of America. The authors wish to gratefully thank Prof. Sergio Brena for valuable discussions, Mr. Mark Gauthier for his assistance in the laboratory, and Mr. Dave Follette and Dr. Fani Derveni for their assistance in manufacturing the metallic auxetic lattices.

References

[1] T. Wangler, E. Lloret, L. Reiter, N. Hack, F. Gramazio, M. Kohler, M. Bernhard, B. Dillenburger, J. Buckli, N. Roussel, R. Flatt, Digital concrete: Opportunities and challenges, RILEM Tech. Lett. 1 (2016) 67–75.
[2] A. Mirmiran, M. Shahawy, Dilation characteristics of confined concrete, Mech. Cohesive-Frict. Mater. 2 (1997) 237–249.
[3] F.E. Richart, A. Brandtzaeg, R.L. Brown, A study of the failure of concrete under combined compressive stresses, Mech. Cohesive-Frict. Mater. 2 (1928) 237–249.
[4] Q. Chen, B. Andrawes, Cyclic stress-strain behavior of concrete confined with NiTiNb-Shape memory alloy spirals, ASCE J. Struct. Eng. 143 (2017) 04017008.
[5] D.C. Kent, R. Park, Flexural members with confined concrete, ASCE J. Struct. Div. (1971) 1969–1990.
[6] S. Sheikh, S.M. Uzumeri, Strength and ductility of tied concrete columns, ASCE J. Struct. Div. (1980) 1079–1102.
[7] B.D. Scott, R. Park, M.J.N. Priestley, Stress-strain behavior of concrete confined by overlapping hoops at low and high strain rates, ACI J. 79–2 (1982) 13–27.
[8] R. Park, M.J.N. Priestley, W.D. Gill, Ductility of square-confined concrete columns, ASCE J. Struct. Div. 108 (1982) 929–950.
[9] J.B. Mander, M.J.N. Priestley, R. Park, Theoretical stress-strain model for confined concrete, ASCE J. Struct. Eng. 114 (1988) 1804–1826.
[10] S.A. Sheikh, S.M. Uzumeri, Analytical model for concretee confinement in tied columns, ASCE J. Struct. Eng. 108 (1982) 2703–2722.
[11] B. Andrawes, S. Moochul, Seismic retrofitting of bridge columns using shape memory alloys, in: Active and Passive Smart Structures and Integrated Systems, 2008.
[12] S. Moochul, B. Andrawes, Experimental investigation of actively confined concrete using shape memory alloys, Eng. Struct. 32 (2010) 656–664.
[13] Q. Chen, B. Andrawes, Plasticity modeling of concrete confined with NiTiNb shape memory alloy spirals, Structures 11 (2017) 1–10.
[14] A. Gholampour, T. Ozbakkaloglu, Understanding the compressive behavior of shape memory alloy (SMA)-confined normal- and high-strength concrete, Compos. Struct. 202 (2018) 943–953.

[15] R.S. Lakes, Design considerations for materials with negative Poisson's ratios, J. Mech. Des. 115 (1993) 696–700.
[16] F. Scarpa, P.J. Tomlin, On the transverse shear modulus of negative Poisson's ratio honeycomb structures, Fatigue Fract. Eng. Mater. Struct. 23 (2000) 717–720.
[17] J.B. Choi, R.S. Lakes, Fracture toughness of re-entrant foam materials with a negative Poisson's ratio: Experiment and analysis, Int. J. Fract. 80 (1996) 73–83.
[18] F. Song, J. Zhou, X. Xu, Y. Xu, Y. Bai, Effect of a negative Poisson ratio in the tension of ceramics, Phys. Rev. Lett. 100 (2008) 245502.
[19] S. Mohsenizadeh, R. Alipour, M.S. Rad, A.F. Nejad, Z. Ahmad, Crashworthiness assessment of auxetic foam-filled tube under quasi-static axial loading, Mater. Des. 88 (2015) 258–268.
[20] T. Li, L. Wang, Bending behavior of sandwich composite structures with tunable 3D-printed core materials, Compos. Struct. 175 (2017) 46–57.
[21] R.S. Lakes, K. Elms, Indentability of conventional and negative Poisson's ratio foams, J. Compos. Mater. 27 (1993) 1193–1202.
[22] K.L. Alderson, V.R. Simkins, V.L. Coenen, P.J. Davies, A. Alderson, K.E. Evans, How to make auxetic fibre reinforced composites, Phys. Status Solidi b 242 (2005) 509–518.
[23] A. Bezazi, F. Scarpa, Tensile fatigue of conventional and negative Poisson's ratio open cell PU foams, Int. J. Fatigue 31 (2009) 488–494.
[24] A. Shanian, F.X. Jette, M. Salehii, M.Q. Pham, M. Schaenzer, G. Bourgeois, K. Bertoldi, A. Gross, F. Javid, D. Backman, Application of Multifunctional Mechanical Metamaterials, Adv. Energy Mater. (2019) 1900084.
[25] L.J. Gibson, M.F. Ashny, G.S. Schajer, C.I. Robertson, The mechanics of two-dimensional cellular materials, Proc. R. Soc. Lond. Ser. A Math. Phys. Eng. Sci. 382 (1982) 25–42.
[26] R. Lakes, Foam structures with a negative Poisson's ratio, Science 235 (1987) 1038–1041.
[27] C.W. Smith, J.N. Grima, K. Evans, A novel mechanism for generating auxetic behaviour in reticulated foams: Missing rib foam model, Acta Mater. 48 (2000) 4349–4356.
[28] L.V. Gibiansky, O. Sigmund, Multiphase composites with extremal bulk modulus, J. Mech. Phys. Solids 48 (2000) 461–498.
[29] Q. Wang, J.A. Jackson, Q. Ge, J.B. Hopkins, C.M. Spadaccini, N.X. Fang, Lightweight mechanical metamaterials with tunable negative thermal expansion, Phys. Rev. Lett. 117 (2016) 175901.
[30] H. Xu, A. Farag, D. Pasini, Multilevel hierarchy in bi-material lattices with high specific stiffness and unbounded thermal expansion, Acta Mater. 134 (2017) 155–166.
[31] J. Hiller, H. Lipson, Tunable digital material properties for 3D voxel printers, Rapid Prototyp. J. (2010).
[32] K. Wang, Y.-H. Chang, Y. Chen, C. Zhang, B. Wang, Designable dual-material auxetic metamaterials using three-dimensional printing, Mater. Des. 67 (2015) 159–164.
[33] R. Jhaver, H. Tippur, Processing, compression response and finite element modeling of syntactiv foam based interpenetrating phase composite (IPC), Mater. Sci. Eng. A 499 (2009) 507–517.
[34] L.D. Wegner, L.J. Gibson, The mechanical behaviour of interpenetrating phase composites - II: A case study of a three-dimenionally printed material, Int. J. Mech. Sci. 42 (2000) 943–964.
[35] L.D. Wegner, L.J. Gibson, The mechanical behaviour of interpenetrating phase composites - III: Resin-impregnated porous stainless steel, Int. J. Mech. Sci. 43 (2000) 1061–1072.
[36] Z. Poniznik, V. Salit, M. Basista, D. Gross, Effective elastic properties of interpenetrating phase composites, Comput. Mater. Sci. 44 (2008) 813–820.
[37] L. Wang, J. Lau, E.L. Thomas, M.C. Boyce, Co-continuous composite materials for stiffness, strength and energy dissipation, Adv. Mater. 23 (2011) 1524–1529.
[38] J.H. Lee, L. Wang, M.C. Boyce, E.L. Thomas, Periodic bicontinuous composites for high specific energy absorption, Nano Lett. 12 (2012) 4392–4396.
[39] O. Al-Ketan, R.K.A. Al-Rub, R. Rowshan, Mechanical properties of a new type of architected interpenetrating phase composite materials, Adv. Mater. Technol. 2 (2017) 1600235.
[40] N. Dukhan, N. Rayess, J. Hadley, Characterization of aluminum foam-polypropylene interpenetrating phase composites: Flexural test results, Mech. Mater. 42 (2010) 134–141.
[41] B. Salazar, P. Aghdasi, I.D. Williams, C.P. Ostertag, H.K. Taylor, Polymer lattice-reinforcement for enhancing ductility of concrete, Mater. Des. 196 (2020).
[42] T. Li, Y. Chen, L. Wang, Enhanced fracture toughness in architected interpenetrating phase composites by 3D printing, Compos. Sci. Technol. 167 (2018) 251–259.
[43] T. Li, Y. Chen, Z. Hu, L. Wang, Exploiting negative Poisson's ratio to design 3D-printed composites with enhanced mechanical properties, Mater. Des. 142 (2018) 247–258.
[44] C. Zmuda, Design of Structural Composite with Auxetic Behavior (WPI thesis), 2017.
[45] X.-T. Wang, X.-W. Li, L. Ma, Interlocking assembled 3D auxetic cellular structures, Mater. Des. 99 (2016) 467–476.
[46] Q.-S. Yang, W. Becker, Numerical investigation for stress, strain and energy homogenization of orthotropic composite with periodic microstructure and non-symmetric inclusions, Comput. Mater. Sci. 31 (2004) 169–180.
[47] EOS, EOS Stainless Steel PH1 for EOSINT M 270 Material data sheet, EOS GmbH, 2018.
[48] ASTM International, ASTM C109/C109M-16a, Standard Test Method for Compressive Strength of Hydraulic Cement Mortars (Using 2-in. or [50-mm] Cube Specimens), ASTM West Conshohocken, PA, USA, 2016.
[49] J.C. Arteaga-Arcos, O.A. Chimal-Valencia, H.T. Yee-Madeira, S. Diaz de la Torre, The usage of ultra-fine cement as an admixture to increase the compressive strength of portland cement mortars, Constr. Build. Mater. 42 (2013) 152–160.
[50] S.J. Foster, M.M. Attard, Experimental tests on eccentrically loaded high strength concrete columns, ACI Struct. J. 94 (1997).
[51] H.-O. Shin, K.-H. Min, D. Mitchell, Confinement of ultra-high-performance fiber reinforced concrete columns, Compos. Struct. 176 (2017) 124–142.
[52] H.-O. Shin, K.-H. Min, D. Mitchell, Uniaxial behavior of circular ultra-high-performance fiber-reinforced concrete columns confined by spiral reinforcement, Constr. Build. Mater. 168 (2018) 379–393.
[53] J.J. Lubliner, S. Oliver, E. Oller, T. OnateLi, A plastic-damage model for concrete, Int. J. Solids Struct. 25 (1989) 229–326.